Optical gratings formed in thin smectic films frustrated on a single crystalline substrate

Jean-Philippe Michel and Emmanuelle Lacaze*
Groupe de Physique des Solides, Universités Paris 6 et 7, UMR CNRS 7588, Campus Boucicaut, 140 rue de Lourmel, F-75015 Paris, France

Michel Alba
Laboratoire Léon Brillouin, UMR CEA-CNRS 12, CEA-Saclay, F-91191 Gif-sur-Yvette Cedex, France

Marc de Boissieu
Laboratoire de Thermodynamique et Physicochimie Métallurgiques, Institut National Polytechnique de Grenoble, Boîte Postale 75, F-38402 Saint Martin d'Hères, France

Marc Gailhanou
LURE, Batiment 209D, Université Paris–Sud, F-91405 Orsay Cedex, France

Michel Goldmann
Laboratoire des Objets Complexes et Interfaces d'Intérêt Biologique, Université Paris 5, FREE CNRS 2303, 45 rue des Saints Pères, Paris Cedex 6, France
and LURE, Batiment 209D, Université Paris–Sud, F-91405 Orsay Cedex, France
(Received 4 December 2003; published 30 July 2004)

Through the combination of three different, complementary techniques (optical microscopy, x-ray diffraction and atomic force microscopy), we reveal the deformations inside thin smectic films frustrated between two interfaces imposing antagonistic anchorings. We study the model system, 4-*n*-octyl-4′-cyanobiphenyl (8CB) between MoS_2 and air, which is characterized by the competition between homeotropic anchoring at air and planar unidirectional anchoring on the substrate, with thicknesses varying around 0.3 μm. Optical microscopy and x-ray diffraction demonstrate the continuous topology of smectic layers between the interfaces, which are stacked into periodic flattened hemicylinders. These latter are one-dimensional (1D) focal conic domains which form an optical grating in the smectic film, of a period ranging from 1 to 2.5 μm. The interpretation of our results through an energetic model, associated with the atomic force microscopy (AFM) measurements, shows the presence below a critical thickness of a new type of curvature wall between neighboring hemicylinders.

DOI: 10.1103/PhysRevE.70.011709 PACS number(s): 61.30.Jf, 61.30.Pq, 61.10.−i, 68.37.Ps

I. INTRODUCTION

During the two last decades many liquid crystals have been intensively studied to develop, in particular, displays and sensing devices. Progress in these applications depends strongly on a good comprehension of the behavior of liquid crystals in different specific confined geometries, characterized by a strong influence of the two interfaces limiting the liquid crystal film. Such an influence is particularly important when the two interfaces induce different anchorings, the associated frustration relaxing through the creation of defects. The increasing technological interest associated with thin objects requires a precise understanding of the nature of these defects. From a more general point of view, the study of liquid crystalline defects in thin films concerns the evolution of soft matter structures in confined geometries, a subject still largely unexplored unlike the case of hard matter structures.

In this framework, we study the liquid crystal 4-*n*-octyl-4′-cyanobiphenyl (8CB) from the *n*-cyanobiphenyles series, on a MoS_2 single crystalline substrate. The aim of this paper is to describe the deformation of a thin smectic-*A* film frustrated by two antagonistic anchorings, planar and nondegenerate on the substrate, homeotropic at the liquid crystal/air interface.

In energetic arguments, Williams and Kleman describe the evolution of the deformations of smectic layers when the curvature angle imposed on the smectic layers increases [1]. In cases of small curvature angles, simple curvature walls are created. When this curvature angle is increased, simple curvature walls first transform into curvature walls mixed with edge dislocations, then into curvature walls with giant edge dislocations. When the curvature angle becomes larger than 20–30°, the defects finally turn into focal conic domains. In the case of small curvatures, curvature walls have been only evidenced in lyotropic systems [2], whereas they are observed in smectic-*C* in case of chevron structures [3,4]. In the case of opposite disorientations, for curvatures close to 180°, curvature walls have been observed through optical microscopy measurements [5] and analyzed as local nematic areas, nematic grain boundaries (NGB). Williams and Kleman, studying the evolution of defects, the curvature angle being induced by the shearing of glass plates limiting the smectic film, have observed giant dislocations followed by

*Electronic address: lacaze@gps.jussieu.fr

focal conic domains as the curvature increases. Chevron structures observed in smectic *A* occur through the formation of focal conics [6]. In the case of antagonistic anchorings at both interfaces leading to curvature angles close to 90°, with degenerate planar anchoring on the substrate, hexagonal networks of focal conics have been described [7,8]. In the case of lyotropic films between a glass substrate and a sponge phase, the network has been described as a mixing of curvature walls and focal conic domains [2,9]. The $8CB/MoS_2$ system differs by a nondegenerate anchoring on the substrate. In a similar geometry with treated glass surfaces instead of MoS_2, x-ray diffraction measurements have been interpreted in terms of the presence of a disordered layer, joining two homogeneous volumes of smectic layers with perpendicular orientations [10,11], instead of focal conics. In addition, most of the previous studies have been performed on films several tens of microns thick. The system's elasticity limit, estimated between 0.1 and several microns then brings a new constraint to the system [2,12] for thin films. In this context we study the deformations of smectic layers for thicknesses smaller than 0.5 μm, in a geometry defined by strong antagonistic anchorings, homeotropic and planar unidirectionnal, leading to a 90° curvature, with a free interface (liquid crystal/air) in front of a solid one (liquid crystal/substrate).

As in the case of treated glass as a substrate, we take advantage of the layering structure of the smectic film to perform x-ray diffraction measurements. Indeed, the use of a single crystalline substrate, which orders the anchored smectic layers, allows a direct exploration by diffraction of the deformations of the smectic layers. Combining this technique with atomic force microscopy (AFM) and optical microscopy, we determine the structure of the frustrated 8CB film, and demonstrate the formation of optical gratings.

The outline of this paper is as follows: in Sec. II we describe the system and the experimental setup. The system's geometry and the anchorings of smectic layers are presented in Sec. III. The film's structure and rotation of smectic layers are demonstrated by the combination of x-ray diffraction (Sec. IV) and optical microscopy (Sec. V). We discuss in Sec. VI the different energetical contributions. Section VII is devoted to the study by AFM.

II. DESCRIPTION OF EXPERIMENTS

The system is composed of a single crystalline substrate molybdenum disulfide MoS_2 and the thermotropic liquid crystal 4-*n*-octyl-4′-cyanobiphenyl 8CB. MoS_2 natural single crystals are coming from Queensland and are supplied by Ward's, N.Y. MoS_2 is a lamellar compound easily cleaved, revealing a clean surface parallel to the basal planes. This surface is composed of ordered sulfur atoms with a hexagonal symmetry ($a_{MoS_2}=3.16$ Å), and a mosaicity lower than 0.02° as checked by x-ray diffraction. The liquid crystal 8CB is a product of BDH (Germany) used without any further purification. It is thermotropic and has a smectic phase in bulk between 21°C and 33.5°C. A 0.1 mol/l concentration solution of 8CB dissolved in chloroform is deposited by spin coating at a speed varying between 1000 and 6000 rpm on a freshly cleaved surface of MoS_2. The sample is then annealed at 80°C for 30 min. The film thickness, checked by optical microscopy, is controlled by the spin speed: for example, 0.3 μm corresponds to a spin speed of 2000 rpm.

X-ray diffraction experiments are performed on D2AM (ESRF, Grenoble, France) and H10 (LURE, Orsay, France) beam lines. Due to the small amount of matter associated with the small thicknesses, the use of synchrotron sources and their high beam brilliance is necessary. The energy is fixed at 8 keV, the beam spot is defined by a pair of slits, so that the beam width is about 500 μm. Its intensity is monitored by a diode. The scattered intensity is scanned by a solid-state detector (NaI). We take advantage of the periodic character of the smectic-*A* phase and detect the wave vector modulus q_s corresponding to the 8CB smectic bulk period. The orientation of the smectic layers is then determined by following the orientation of this $\vec{q}_s$ vector with respect to the interfaces.

Optical microscopy experiments are performed with a polarizing microscope Leica DMR fitted with a color camera connected to a PC for acquisition. Optical microscopy images are obtained in the reflection mode, due to the MoS_2's opacity.

Atomic force microscopy experiments are performed on a Nanoscope III microscope (Veeco) with commercial silicon tips. Their radius is estimated by the manufacturer to be 100 nm. This technique allows the study of the liquid crystal/air interface. Due to the soft character of 8CB, we work in the Tapping mode at scan frequencies from 0.5 to 1 Hz. Image size varies from 1 to 100 μm. Careful examination of our approach-retract curves shows the existence of a narrow working range associated with setpoint variations of 4 nm, close to the highest possible setpoint value. This working range allows the visualization of the 8CB/air interface without damage to the surface, contrary to the lower setpoint values, suggesting that we work in non-contact regime. This interpretation is supported by recent AFM studies on liquid crystalline materials, in particular 8CB [13], demonstrating how it is possible to measure forces as weak as 10^{-10} N with the AFM tip inside the liquid crystal film in nematic and smectic phases. Such results show that an AFM tip can easily penetrate a smectic film in the case of contact during each oscillating cycle of the Tapping mode.

III. ANCHORING

Before studying the bulk topology of smectic layers, we have to determine the anchoring nature close to the interfaces. First of all, the liquid crystal/air interface imposes a well known homeotropic anchoring [7,14] (the average 8CB molecular direction is perpendicular to the interface and the smectic layers are then parallel to it). It has been previously demonstrated that, after annealing, the MoS_2/liquid crystal interface under the smectic bulk is formed by adsorbed molecules stacked in straight ribbons, organized in a two-dimensional (2D) crystal, commensurate with respect to the MoS_2 network [15–20]. In this bidimensional network, 8CB molecules lie flat on the substrate surface. If such a planar molecular configuration is preserved close to the MoS_2 sur-

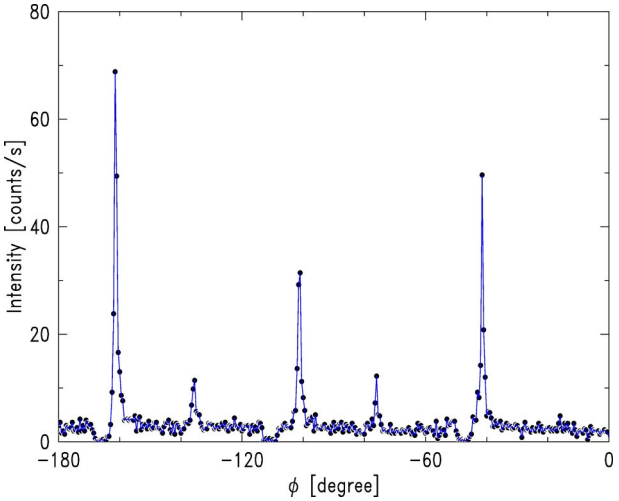

FIG. 1. Grazing incidence diffraction profile obtained by an azimuthal scan on a sample of thickness 0.4 μm, for $q=0.2$ Å^{-1}. The different Bragg peaks correspond to the different anchoring directions of perpendicular smectic layers. The pronounced dips at −165.5°, −111°, and −45.5° correspond to the furnace Tungsten pillars passing either in the direct beam or in front of the detector.

face, a planar anchoring is induced and therefore one expects the formation of perpendicularly anchored smectic layers on the substrate surface.

We have recently determined the anchoring properties of 8CB on MoS_2 by combining scanning tunneling microscopy, optical microscopy, and x-ray diffraction experiments [21]. X-ray diffraction used in grazing incidence is a particularly appropriate implement to study a planar anchoring, since it allows the specific exploration of smectic layers perpendicular to the substrate. The sample is set in a grazing incidence configuration where the beam spot reaches the lower interface through the 8CB bulk at an incidence of about 0.3°, comparable to the MoS_2 critical angle but higher than the one in the 8CB bulk. The detector position is moved in the substrate plane to probe the smectic wave vector modulus $q_S=0.2$ Å^{-1} [22]. Due to the grazing incidence geometry, the transfer wave vector is nearly parallel to the substrate's surface and smectic layers almost perpendicular to the substrate surface are specifically detected. Keeping the incidence angle and the detector position constant, the sample is rotated over 180°.

Such a scan provides an intensity profile versus the azimuthal angle. Figure 1 shows the evidence of five distinct Bragg peaks with different intensities and full width at half maximum (FWHM) of the order of 0.5°. This result, which indicates the presence of smectic layers perpendicularly anchored on the substrate, confirms the planar nature of the anchoring on the MoS_2 surface. Moreover, the intensity vanishes between the peaks which indicates that only few anchoring directions are present on the substrate. Five types of domains characterized by a unidirectionnal anchoring are formed on this sample. The Bragg peak intensities are not all identical. These intensity differences indicate that the domains are not homogeneously distributed in the area illuminated by the incident beam and seen by the detector. Differences in the relative proportions of the allowed anchoring directions are due to the fact that the domains size, from several tens to several hundreds of microns, is of the order of the beam size, 500 μm in the case of the experiment associated with Fig. 1. Actually, by combining the results obtained on several different samples, we have detected six different anchoring directions, along which perpendicular smectic layers can be anchored, at ±17.5° and ±17.5°±60° away from the [100] MoS_2 direction. These values, related to the nature of the underlying bidimensional network, are discussed elsewhere [21].

In each domain associated with a unique given anchoring direction, antagonistic anchorings occur, homeotropic at one interface and planar, nondegenerate, at the other interface.

IV. EXPERIMENTAL STUDY OF FILM STRUCTURE BY X-RAY DIFFRACTION

A. Experimental configuration

We now address the film structure between both interfaces in contact with the MoS_2 surface and air. It has been measured by x-ray diffraction on samples of thickness 0.4 and 0.45 μm, leading to similar results. In order to explain the topological connection between the perpendicular layers and the parallel ones, we select one anchoring direction of perpendicular layers by choosing and keeping constant the corresponding azimuthal angle value. In such a configuration, we explore only the domains associated with this anchoring direction and therefore all the layers oriented in that direction diffract.

The scattered intensity is measured by rotating the $\vec{q}_S$ vector continuously, from a parallel orientation with respect to the MoS_2 surface to a perpendicular one, keeping the absolute value of the $\vec{q}$ vector constant during the scan ($q_S=0.2$ Å^{-1}). Such a motion is obtained by varying the beam incidence angle between 0° and 1.4° and varying as well the position of the detector. The diffraction plane changes from a grazing incidence configuration where perpendicular layers are investigated, to a q_Z symmetrical one with equal incident and exit angles (fixed by the q_S value, $\theta_I=\theta_E=1.4°$) where parallel layers are investigated. We denote α the angle of the $\vec{q}$ vector with respect to the sample plane. The $\vec{q}_S$ vector being parallel to the director of the smectic layers, such a motion allows the study of the different orientations of the layers.

B. Raw and corrected profiles

Intensity versus α is plotted in Fig. 2 for a 8CB film of thickness 0.45 μm. At $\alpha=0°$ the vertically anchored layers are measured, whereas at $\alpha=90°$ the parallel ones are investigated. The curve marked by the gray line is a scan locked on the selected anchoring direction of smectic layers, obtained at 25°C in the smectic phase. It is compared to the same scan obtained at 35°C in the nematic phase and to a scan obtained at 25°C but locked on an azimuthal direction disoriented at 5° away from the selected anchoring direction.

The upper curve (gray line) shows that the intensity is almost constant between $\alpha=15°$ and $\alpha=80°$: this is the main result. The slight decrease of intensity in this interval reflects

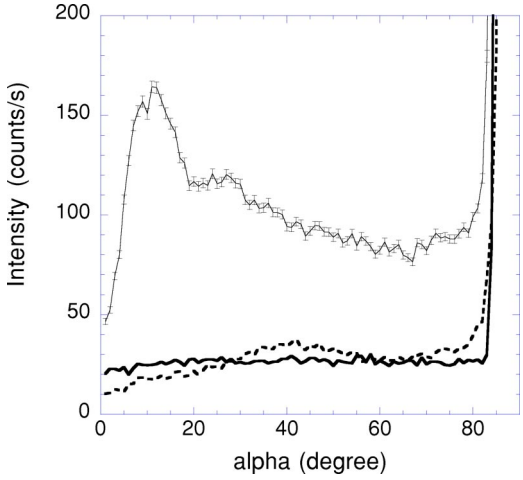

FIG. 2. Raw intensity profile versus α, obtained on a sample of thickness 0.45 μm. Gray line: at 25°C in smectic phase, locked on the selected anchoring direction, error bars corresponding to statistical error; dotted black line: at 35°C in the nematic phase, locked on the same anchoring direction; black line: at 25°C, locked on a direction disoriented at 5° away from the selected anchoring direction.

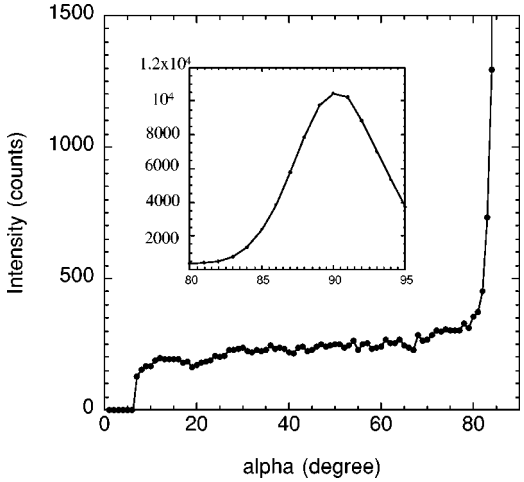

FIG. 3. Intensity profile versus α, obtained after corrections (background noise, footprint evolution, transmission corrections, and intensity set to zero below the 8CB/air critical angle) performed on the scan of Fig. 2. The inset corresponds to a zoom on the intensity values around $\alpha=90°$.

the evolution of the beam footprint, i.e., the evolution of the area illuminated by the incident beam and seen by the detector. This area is smaller than the sample size and decreases regularly with increasing α. A wide intensity increase at small angles corresponds to the beam penetration into the smectic bulk associated with the Yoneda peak [23], when the incidence angle goes beyond the 8CB/air critical angle (0.17°). The 8CB critical angle value corresponds to an orientation of the $\vec{q}$ vector equal to $\alpha=7°$ with respect to the sample plane. Below this critical angle, the incident beam is totally reflected and the intensity is negligible.[1] The strong increase of intensity close to $\alpha=90°$ is mainly due to the MoS_2 reflectivity, since the geometry becomes specular and symmetric for the wave vector.

The background noise is measured in the nematic phase at the temperature T=35°C. The corresponding curve is plotted with a dotted black line in Fig. 2. In order to avoid the MoS_2 reflectivity, the background noise can be subtracted from the raw data.

The misoriented scan (black line in Fig. 2) shows that the intensity becomes equivalent to the background noise intensity when the scan is performed in a direction disoriented from the anchoring direction. This result demonstrates that, for a given domain, the layers director strictly remains in the rotation plane of the $\vec{q}$ vector, as defined by the anchoring direction on the substrate.

As described above, corrections must be performed to the measured intensity profiles. Background is subtracted. The evolution of the beam footprint is taken into account through a geometrical correction term. A transmission correction takes into account the transmission factor associated with the Yoneda peak. We set to zero all intensity below the 8CB critical angle [23,24].

[1]Actually, an evanescent wave, propagating parallel to the upper interface, always exists in the 8CB bulk.

The result is presented in Fig. 3. A continuous intensity profile, almost constant from $\alpha=10°$ to $\alpha=80°$, is obtained. The broad asymmetry, corresponding to the penetration of the incident beam in the smectic bulk and to the footprint evolution, has disappeared. We verified that similar intensity profiles are obtained for other anchoring directions.

Radial and tangential extensions of the intensity distribution have been measured. Figure 4 shows a radial scan obtained at $\alpha=40°$. The scan is centered at $q_S=0.2$ Å^{-1}, as well as the radial scans associated with any value of α. This demonstrates that the smectic period is well preserved, whatever the layer deformations. Such scans are limited by the angular resolution but indicate a coherence length larger than 100 Å. Figure 5 shows a tangential scan performed at the angle $\alpha=15°$, through a variation of the azimuthal angle defined by the anchoring direction. The in-plane mosaicity is 0.39°. Typically, this value is one order of magnitude higher than the MoS_2 surface mosaicity (0.02°), due to the soft nature of the smectic phase. This value is of the same order as the mosaicity of smectic layers of a different smectic compound oriented by a magnetic field of 1 T [25]. This demonstrates that smectic layers are well oriented by the anchoring on the underlying single crystal, in particular when compared to gratings on glass or silicon which induce a mosaicity higher by one to two orders of magnitude [10].

C. Interpretation

The film structure has to be consistent with the two main characteristics of the x-ray diffraction data: (i) a constant diffracted intensity, i.e., a homogeneous distribution of diffracting smectic layers when the director rotates from 10° to 80°, (ii) the strict confinement of the smectic layer director in the plane perpendicular to that of the sample and imposed by the selected planar anchoring direction.

The confinement of the layer director is incompatible with a discontinuous structure composed of a disordered middle

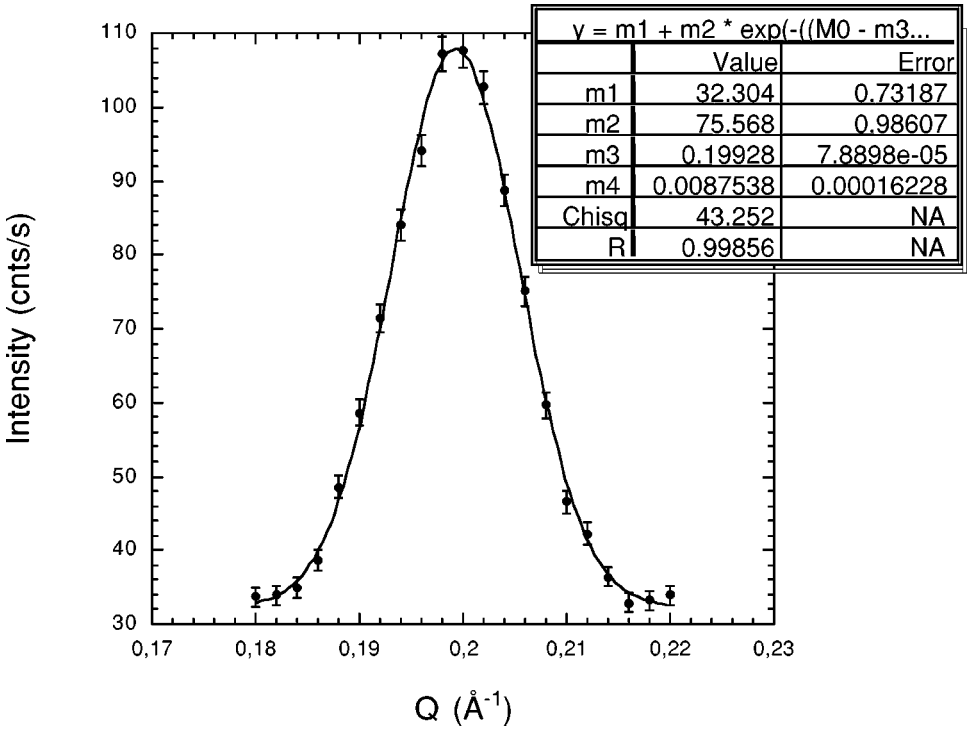

FIG. 4. Radial scan performed on a sample of thickness 0.45 μm at $\alpha=40°$. The fit data indicate a maximum at the 8CB wave-vector modulus 0.2 $Å^{-1}$. The width is equal to 0.08 $Å^{-1}$. It is defined by the experimental angular resolution and demonstrates a coherence length larger than 100 Å.

layer separating two smectic volumes with orthogonal orientations, as proposed in a similar frustrated system [10,11]. Such a discontinuous structure should lead to a constant intensity profile not only in the case of an α scan (except at the angles 0° and 90°), but also along any azimuthal direction. This argument is in contradiction with the scan at 25°C, locked on a direction disoriented by 5° (Fig. 2), as well as with the tangential scan at the angle $\alpha=15°$ (Fig. 5).

Moreover, the constant intensity range between $\alpha=10°$ and $\alpha=80°$ does not agree with the presence of curvature walls in the bulk, sharing layer sets of different orientations. In such a discontinuous structure, the strong discontinuity in the layers should provide a null intensity at the angles between the layer set orientations, as in case of chevrons structures [6]. Such a discontinuous structure cannot produce a constant intensity profile between $\alpha=10°$ and $\alpha=80°$.

Actually, only a continuous structure, in which smectic layers turn continuously between the two interfaces, can satisfy both characteristics. Such a continuous rotation of layers can be understood in a cylindrical geometry (Fig. 6) which corresponds to the observed confinement of the smectic director as well. A concentric stacking of smectic layers in a half cylinder lying flat on the substrate provides a constant number of diffracting layers when the director rotates from 0° to 90°. The corresponding cylinder axis is perpendicular to the rotation plane of the smectic layers and is parallel to the substrate. It can be considered as a 1D focal conic, transformed into a line parallel to the substrate and to the anchor-

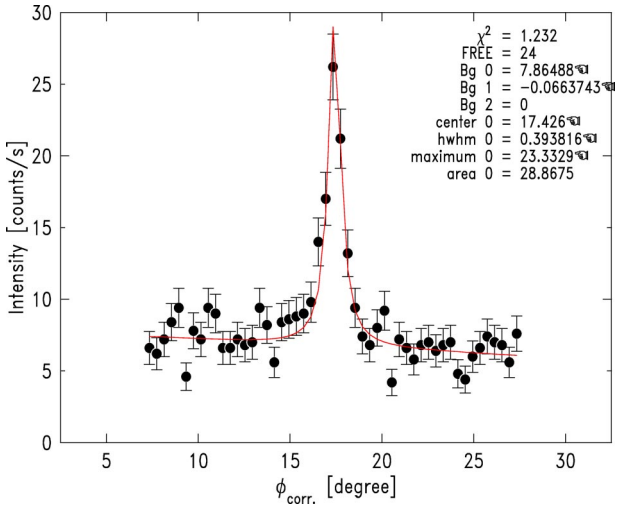

FIG. 5. Tangential scan executed on a sample of thickness 0.4 μm at $\alpha=15°$. It shows that rotating smectic layers are well oriented with an in-plane mosaicity of 0.39°.

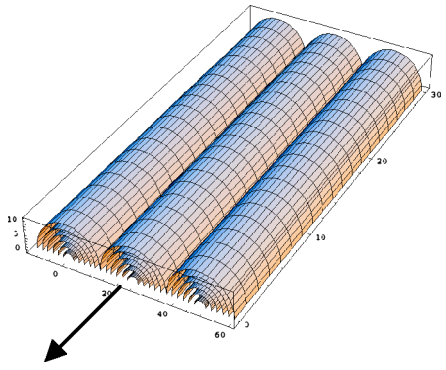

FIG. 6. Continuous structure compatible with intensity profiles measured by x-ray diffraction. Smectic layers are concentrically stacked into hemicylindrical structures lying flat on the substrate, and turn continuously from a perpendicular anchoring on the substrate to a parallel one at the liquid crystal/air interface. The defect is a line, located along the arrow.

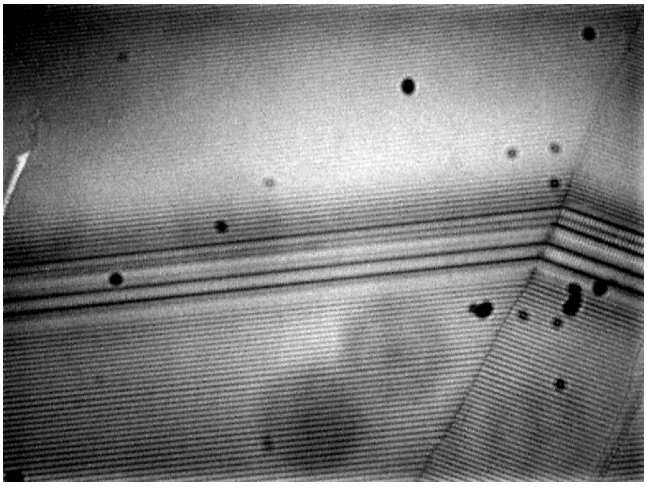

FIG. 7. Optical microscopy image between crossed polarizers of size 165 μm $\times$ 123 μm obtained on a sample of thickness 0.20 μm. The central lines, which appear darker in the middle of the image, correspond to a thicker region.

ing direction of smectic layers on the substrate. Such a result confirms that, for high disorientation angles, focal conic domains should prevail regarding curvature walls [1], even for thicknesses as small as 0.45 μm. Similar cylindrical deformations had been previously suggested in case of thick smectic-*C* films frustrated by the same anchorings, in order to interpret optical microscopy measurements [26].

Finally, in a domain of constant thickness the liquid crystal film should form a periodic network of such hemicylinders. Since the period should be twice the radius of the cylinders and since the thickness is equal to the radius of the cylinders, the period should be twice the thickness of the smectic film. Therefore we have performed optical microscopy experiments in order to check such a model obtained through x-ray diffraction measurements.

V. STUDIES BY OPTICAL MICROSCOPY

Figure 7 is an optical microscopy image between crossed polarizers in the reflection mode of a sample of mean thickness 0.20 μm. One observes two distinct domains of different orientations separated by a grain boundary. Typical domains dimensions are in the range 10–100 μm. Each domain is filled with a succession of dark parallel lines. These dark lines can be associated with the linear defect cores of hemicylinders, indicated through an arrow on Fig. 6 (1D focal conics), where smectic directors suffer a strong discontinuity of orientation.

The disorientations between the different domain directions can be measured. From Fig. 7, one obtains 25°. More generally, one systematically obtains ±60°, 35°, 35° ± 60°, 25° and 25° ± 60°, the same values which separate the different Bragg peaks of Fig. 1. The Bragg peaks of Fig. 1 are the signature of the anchoring directions of the smectic layers on the substrate. We have previously demonstrated that each of these anchoring directions is at ±17.5° and ±17.5° ± 60° away from the [100] MoS_2 direction, leading to the formation of domains in the smectic films, associated with one of these six possible anchoring directions [21]. The disorientation between the anchoring directions of two different domains are consequently ±60°, 35° = 2 × 17°, 35° ± 60°, 25° = 60° − 35° and 25° ± 60°. The fact that domains are visible by optical microscopy and that the disorientations between the dark lines correspond to the disorientations between the different possible anchoring directions on the substrate is consistent with a model of smectic layers staked in hemicylinders flat on the substrate. In such a model the linear cores of the hemicylinders are parallel to the part of the smectic layers perpendicularly anchored (planar anchoring) on the substrate (see Fig. 6). In a given domain, all the linear cores should then be parallel and the disorientations of the linear cores of two different domains should be the same than the disorientations of the anchoring directions. The angle 25° = 60 − 2 × 17.5° corresponds to two different anchorings of smectic layers, one at 17.5° away from one crystallographic direction of the substrate, the other one at −17.5° away from another crystallographic direction of the substrate, disoriented by 60° due to the hexagonal symetry of MoS_2. Optical microscopy therefore confirms an organization of well oriented smectic hemicylinders lying flat on the substrate and stacked in domains with different orientations. Such networks correspond to the hexagonal networks of focal conics evidenced in thicker films on water [7], isotropic phase [8], and sponge phase [9] as substrate. Here the network is 1D, due to the nondegenerated anchoring on the substrate.

We can obtain from the optical microscopy observations an experimental curve relating the period between dark lines versus the thickness of the film. Such a measurement is not attainable by x-ray diffraction because of the large value of the period, on the order of 1 μm. We studied samples of different thicknesses, all other experimental parameters being identical. Thicknesses are determined by Newton's tints. Each tint corresponds to an optic delay which can be related to a precise thickness value through a simple relation that includes the 8CB mean refractive index. We have selected homogeneous regions from films of different mean thicknesses. The results are presented in Fig. 8. They were obtained from 55 measurements on domains of thickness varying from 0.09 to 0.45 μm. As expected, a linear increase of the period is obtained with respect to the film thickness. The data can be adjusted by a linear curve of slope of 4.44. Such a value disagrees with the half-cylindrical model, which leads to a slope of 2. However, this result can be understood through an hypothesis of flattenned hemicylinders with flat parts joining two quarters of hemicylinders (Fig. 9). In such a model the flat part is composed of horizontal layers, parallel to the substrate's surface, joining two smectic volumes of rotating layers. Through such an hypothesis, the black line contrast in the optical microscopy images between crossed polarizers correspond to the presence of horizontal layers which form ribbons associated with molecules perpendicular to the polarizers' direction. These ribbons are parallel to the 1D focal conics associated with the flattened hemicylinders, located in the curvature centers of the quarters of hemicylinders, and are still parallel to the anchoring direction of the smectic layers on the substrate (see Fig. 9).

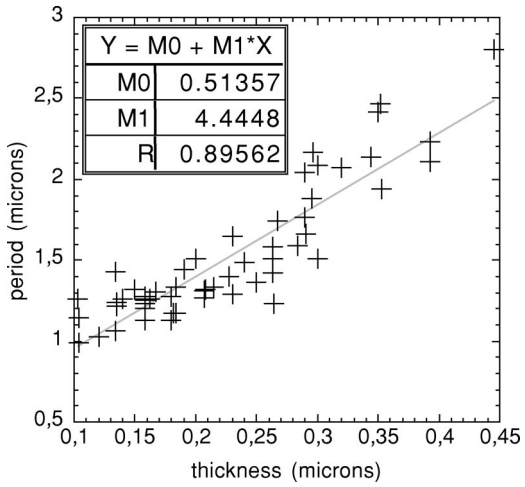

FIG. 8. Evolution of the linear network period observed by optical microscopy versus film's thickness, as measured by Newton's tints. Parameters from a linear fit to the measured points are presented in the inset; they correspond to a slope equal to 4.44.

This hypothesis agrees with the x-ray diffraction results. The Fig. 3 inset shows a stronger intensity at $\alpha=90°$ despite the subtraction of the substrate reflectivity. At $\alpha=90°$, smectic layers parallel to the substrate are diffracting. Note that these layers are degenerated with respect to the azimuthal angle: parallel smectic layers belonging to all domains diffract together and contribute to the measured intensity. In the case of pure hemicylinders forming six types of domains equivalently dispatched on the substrate, the maximum intensity should be equivalent to six times the intensity from rotating layers. In Fig. 3, the intensity at $\alpha=90°$ is 50 times higher than between $\alpha=10°$ and $\alpha=80°$. This high intensity at $\alpha=90°$ is therefore associated with the existence of a large number of parallel layers. Thus, x-ray diffraction agrees with a structure of flattenned hemicylinders with flat layers between the rotating ones. The optical microscopy allows the shape of the periodic structures inside which smectic layers are rotating concentrically to be specified.

VI. DISCUSSION

In order to understand the origin of the flattening, we have built a model describing a single domain with a given orientation and width L. The geometry of the model corresponds to that in Fig. 9 and is presented in Fig. 10.

The domain of width L involves $L/(2r_o+L_o)$ flattenned hemicylinders where r_o is the radius of a hemicylinder and

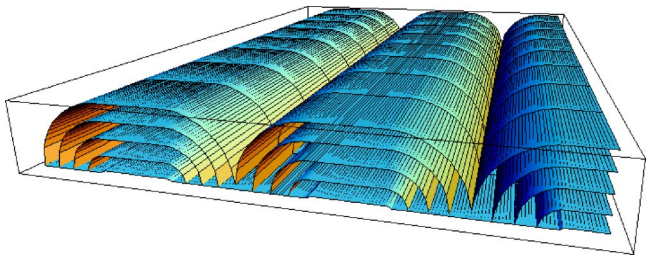

FIG. 9. Scheme of periodic flattenned hemicylinders.

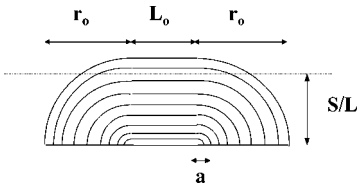

FIG. 10. Geometry of the energetic model composed of flattenned hemicylinders.

L_o the width of the flat part. For a given domain, the total energy per unit length is the sum of four terms:

$$E = E_{S1} + E_{el} + E_{S2} + E_D,$$

$$E = L\left[\gamma_{air}\frac{\pi r_o + L_o}{2r_o + L_o} + \frac{\pi K}{(2r_o + L_o)}\ln\left(\frac{r_o}{a}\right) + \left(\frac{\Delta\gamma_{MoS_2}L_o}{2r_o + L_o} + \gamma_{MoS_2}\right) + \frac{U}{2r_o + L_o}\right].$$

E_{S1} stands for the energy of the 8CB/air interface, where γ_{air} is the 8CB/air surface tension in a homeotropic alignment ($\gamma_{air}=30\times10^{-3}$ J/m^2 [27–29]). The energy cost is associated with the curvature of the rotating layers which imposes a curvature of the upper surface. E_{el} stands for the elastic curvature energy of rotating layers. K is the 8CB curvature modulus in the smectic phase and is equal to 7×10^{-12} J/m [30]. a is the usual cut-off associated with the presence of defects in the area of high curvature (see Fig. 10). E_{S2} stands for the the energy of the 8CB/substrate interface where γ_{MoS_2} is the 8CB/substrate surface tension in a planar anchoring. $\Delta\gamma_{MoS_2}$ represents the variation of the $8CB/MoS_2$ surface tension between an homeotropic and a planar anchoring, i.e., the anisotropy of the $8CB/MoS_2$ surface tension. The cost of such an energy is associated with the flat layers in contact with the substrate. E_D stands for the energy of the two linear cores associated with the cutoff a. U is of the order of K [12,31,32].

We are able to express L_o in terms of r_o, with S the volume per unit length (see Fig. 10),

$$L_o(r_o) = \frac{\pi r_o^2 - 4Sr_o/L}{2(S/L - r_o)}.$$

E can be rewritten as a function of the variable r_o

$$E(r_o) = E_{S1}(r_o) + E_{el}(r_o) + E_{S2}(r_o) + E_D(r_o),$$

$$E(r_o) = L\left[\gamma_{air}\left(\frac{\pi}{4-\pi} + \frac{2S/L(\pi-2)}{(\pi-4)r_o}\right) + \frac{2\pi K(S/L - r_o)}{(\pi-4)r_o^2}\ln\left(\frac{r_o}{a}\right) + \Delta\gamma_{MoS_2}\left(\frac{-\pi}{4-\pi} + \frac{4S/L}{(4-\pi)r_o}\right) + \gamma_{MoS_2} + 2U\left(\frac{S/L - r_o}{(\pi-4)r_o^2}\right)\right].$$

Evaluating the two first terms, one finds that the surface energy E_{S1} dominates: for the measured thickness range, E_{S1} is higher by three orders of magnitude than E_{el} which is of

the same order as E_D. The surface energy in contact with air therefore costs much more than elastic energy. This result illustrates the property of thin films to be led by an energetic competition where surface energies are dominant. The presence of flat areas, composed of stacked parallel layers, allows for a minimization of the 8CB/air surface energy. Competition takes place between the term E_{S1} and the term E_{S2}, the latter depending strongly on extension of the parallel layers. The unknown values are $\Delta\gamma$ and a. Associating the experimental L_o and r_o deduced from the evolution of network period versus thickness (Fig. 8) and the minimization of the free energy versus r_o, we are able to estimate these parameters. One obtains

$$a > r_o e^{[(r_o-3S/L)/2S/L]+2U/(2\pi K)} \sim 0.1\ \mu\text{m}$$

and

$$\Delta\gamma_{MoS_2} = \frac{\pi-2}{2}\gamma_{air} + \frac{2\pi K}{(4S/L)r_o}[r_o - S/L] + [2S/L - r_o] \times\left(\frac{[2\pi K \ln(r_o/a) + 2U]}{(4S/L)r_o}\right) \sim 17.13\times 10^{-3}\ \text{J/m}^2.$$

The a value corresponds to the length associated with the high cost of elastic energy and is generally estimated around 1 μm [2]. 0.1 μm is not so far from the 8CB film thickness, around 0.3 μm, which underlines the fact that, in thin films, defects cannot be neglected. The $\Delta\gamma_{MoS_2}$ appears extremely high compared to most of the anchoring energies of nematic phases, between 10^{-7} J/m^2 and 10^{-4} J/m^2 [33,34], as well as compared to most of the already measured anisotropies of interfacial tensions, 5×10^{-6} J/m^2 for the nematic 5CB/air interface [35], 2.5×10^{-5} J/m^2 for the nematic 8CB/water interface [7], 10^{-5} J/m^2 for a nematic/smectic-B interface [36], and 10^{-5} J/m^2 for a lyotropic smectic/sponge interface [37,38]. However, it is of the same order as the anchoring energy of a smectic/lecithin covered indium-tin-oxyde (ITO), leading homeotropic anchoring, also indirectly obtained through the observation of defects [31]. Figure 11 shows the comparison between experimental and theoretical curves of the period versus the thickness, $P=f(r_o)$. The experimental curve is obtained from optical microscopy data, with r_o corresponding to the thickness as measured through Newton tints observations. The theoretical curve is obtained by the minimization of the free energy for different values of the volume per unit length S, using the previously determined values of a and $\Delta\gamma$. We obtain a positive slope, in agreement with the optical microscopy results. However, the slope is 5 times higher than the experimental one. The model fails to recover the correct evolution of the structures with increasing thickness which can be associated with the non-precisely-known expression of the linear defects energy or to a missing ingredient in the model. To go further in the experimental description of the layers and understand the origin of such a failure, we performed AFM measurements.

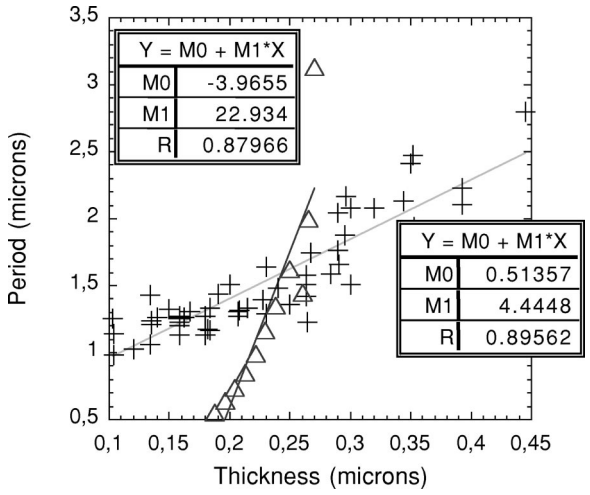

FIG. 11. Comparison between the experimental curve $P=f(r_o)$ resulting from optical microscopy experiments (crosses) and the curve obtained by minimizing the model free energy (triangles). Parameters from a linear fit of the two distributions are presented in the insets; they correspond to a slope equal to 4.44 in case of the optical microscopy experiments (crosses) and to a slope equal to 23 in case of the theoretical curve (triangles).

VII. STUDY BY ATOMIC FORCE MICROSCOPY IN THE TAPPING MODE

Atomic force microscopy (AFM) allows the observation of the upper interface in contact with air and has been already performed on networks of focal conics of cholesteric oligomers [39]. Because a smectic film is soft at ambient temperature, we used the Tapping mode in a noncontact regime. The tip oscillates at a fixed frequency above the free interface without contact.

A. Experimental results

Figure 12 shows an image (size 50 μm) obtained on a sample of thickness 0.3 μm. Each domain presents a periodic network of linear parallel structures whose period is about 1.8 μm. Values of disorientations between domains are in agreement with optical microscopy and x-ray diffraction results. One observes 60° on Fig. 12, but more generally one measures systematically ±60°, 25°, 25°±60°, 35°, or 35°±60°. Moreover, the linear parallel structures in the AFM images correspond to periodic undulations of the upper interface: white areas correspond to bumps and the black ones to hollows. These periodic undulations are fully consistent with the presence of hemicylinders lying flat on the substrate: the upper interface is parallel to the smectic layers and must adopt the same curvature.

From the AFM images we can infer the experimental evolution of the period versus the film's thickness. We studied samples with thicknesses varying from 0.08 to 0.44 μm. Thicknesses have been measured by optical microscopy and checked under the AFM head with the binocular loop. Results are presented in Fig. 13. Periods, as measured by AFM, agree perfectly with those measured by optical microscopy and the two distributions fit the same linear curve. This result

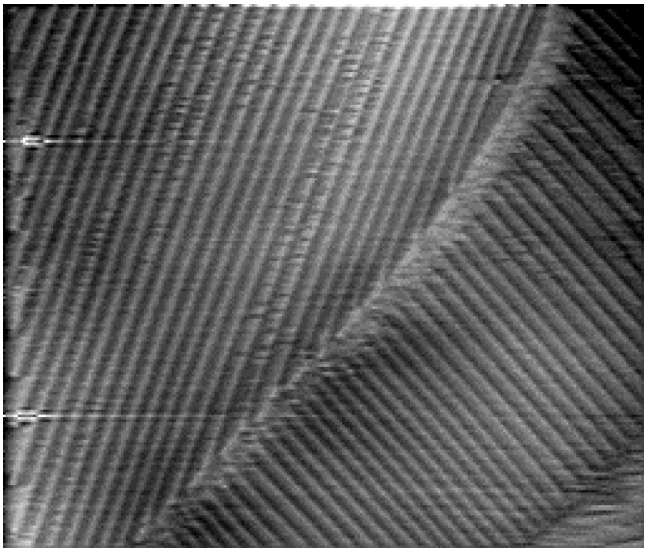

FIG. 12. AFM image obtained on a sample of thickness 0.3 μm. Size: 50 μm.

demonstrates that the same structures are observed by optical microscopy and AFM and that AFM images are not distorded in the horizontal plane: the frustrated film forms an optical grating associated with the presence of undulations at the upper surface and whose period vary from 0.8 to 2.5 μm, depending on the thickness.

The image in Fig. 14(a) is obtained by zooming to enlarge the view of the undulations on a sample 0.13 μm thick. Such an image is in good agreement with the surface of a network of flattened hemicylinders, with flat parts joining rotating ones, as also outlined by the cut in Fig. 14(b). However, measuring the depths between two quarters of cylinders, one obtains 17 nm, 8 times smaller than the value expected, equal to the thickness 0.13 μm.

Measuring the flat extension in Fig. 14(b), one obtains a value of about 350 nm. However, in the frame of flattened hemicylinders, the extension of the flat part L_o can be deduced from the curve $P=f(r_o)$, as obtained from optical microscopy measurements (Fig. 13): in case of $r_o=0.13$ μm, $L_o=0.8$ μm, two times larger than the measured value.

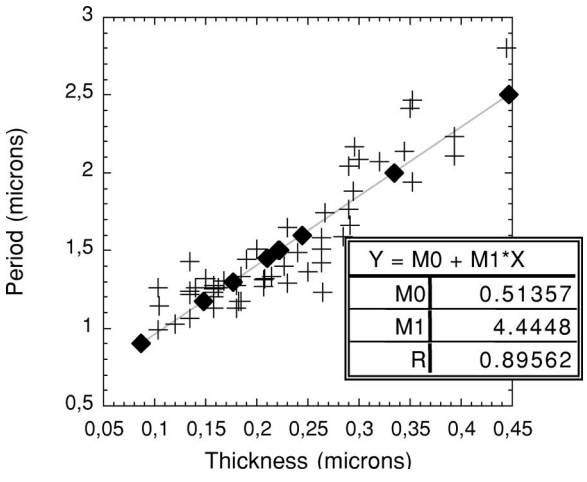

FIG. 13. Comparison between the linear network period measured by optical microscopy (crosses) and by AFM (filled squares) versus thickness. Parameters from a linear fit to all data are presented in the inset; they correspond to a slope equal to 4.44.

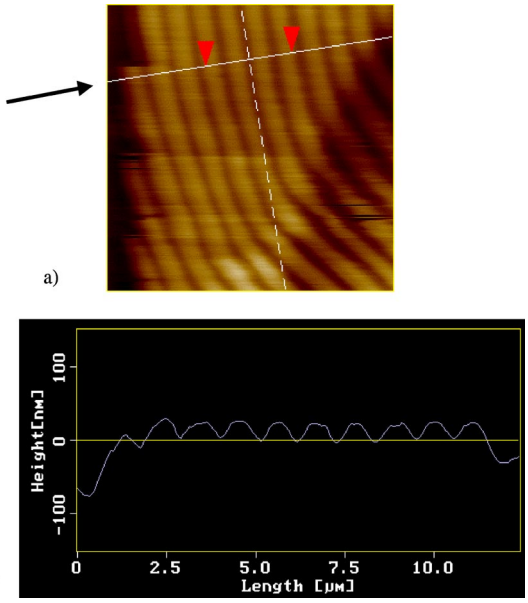

FIG. 14. (a) AFM image obtained on a 0.13 μm thick sample. Image size: 12 μm. (b) Vertical cut executed along the line marked by the arrow.

B. Tip-surface convolution calculus

In order to explain such a disagreement, the role of the tip-surface distance has to be taken into account. Indeed, in the noncontact Tapping mode regime, the tip interacts on a lateral distance equivalent to the tip-surface distance. The tip can then be modeled by a sphere with an effective radius r_p, taking into account the tip's real curvature radius r_c and the tip-surface distance d ($r_p=d+r_c$, see Fig. 15). In such a case, the measured surface of flattened hemicylinders is convo-

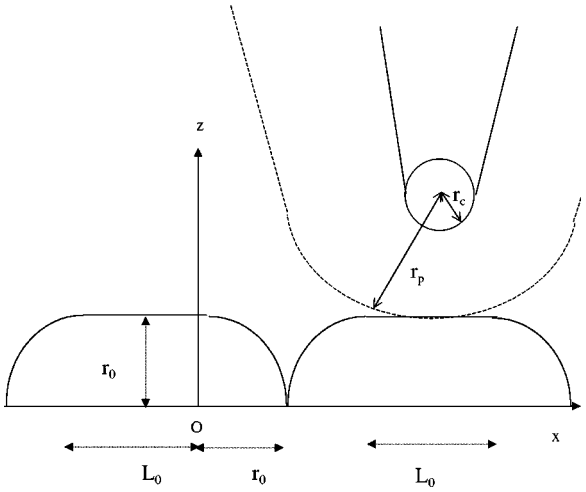

FIG. 15. Scheme of the upper interface's profile interacting with an AFM tip through an interaction extension of the order of the sum of the tip radius and the tip-surface distance.

TABLE I. Evolutions of the depth between hemicylinders with the film thickness.

Thickness in μm	0.15	0.25	0.35
Measured depth in μm	0.011	0.015	0.018
Calculated depth z, in μm, taking into account r_p	0.026	0.06	0.103

luted by the AFM tip. The radius of the curved surface is increased by a value of the order of the effective tip radius. From the AFM image of Fig. 14, one can estimate r_p as equal to $(0.8-0.35)/2=0.22$ μm. With a real tip radius estimated by the manufacturer to be 100 nm, one obtains a tip-surface distance close to 100 nm, which appears reasonable.

However, in order to turn now to measured depths between the hemicylinders, we need to analyze only images with similar tip-surface distances, a value difficult to control in the Tapping mode. Despite the large number of measurements, we then decided to consider only three images leading to the same r_p values ($r_p=0.3$ μm, as deduced from the extension of the flat parts). Table I presents the evolution of the depth between the hemicylinders for three different 8CB film thicknesses. We obtained the apparent depth of the hollow located between the hemicylindrical structures, taking into account a tip-surface distance of 200 nm or an effective tip radius of 300 nm, through a calculation based on Odin's work [40]. The hollow depth z is given by the following formula:

$$z=(r_o+r_p)\left(1-\sqrt{1-\frac{r_o^2}{(r_o+r_p)^2}}\right).$$

Applying this formula to the three thicknesses measured by AFM and indicated in Table I, one obtains depths values clearly larger than the measured ones (see Table I, third line). In order to interpret our results, one has to consider that matter fills the space between the flattened hemicylinders, leading to the presence of defects which accomodate the disorientations between two consecutive flattened hemicylinders.

Focal conics are visible in optical microscopy images between the dark lines for thicknesses higher than 0.35 μm, leading to periodic networks perpendicular to the flattened hemicylinders network but of similar period. Curvature walls are usually divided in linear focal conics in the case of high disorientations [1,31,41]. However, the focal conics abruptly disappear for thicknesses smaller than 0.35 μm. Following Williams and Kleman [1], the focal conic domains between the hemicylinders are replaced by curvature walls, as shown schematically in Fig. 16, possibly mixed with dislocations which remain invisible by optical microscopy [42]. Such a result is related to the small thickness of the samples and to the limited space available between the hemicylinders which would impose too high curvature of the rotating smectic layers for thicknesses smaller than 0.35 μm. The defects schematized in Fig. 16 are curvature walls similar to the curvature walls already observed by Dozov and Durand [5]. However, in this latter case, the layer disorientation remained close to 180° whereas between MoS_2 and air the disorientation varies between 180° and $2\theta_0$ (see Fig. 16). In principle, it should be possible to deduce the θ_0 values from AFM measurements. However the corresponding calculations appear highly dependent on the r_p value, which is only roughly estimated through the flat extension measurements. In any case, the observation of such matter between the hemicylinders appears responsible for the discrepancy between theoretical and experimental curves in Fig. 11. The undulations are finally the result of competing anchoring, rotating, defect, and 8CB/air energies. The presence of the defects between the hemicylinders is clearly due to the high cost of interfacial energy at the 8CB/air interface, which is reduced in the configuration of Fig. 16 compared with the one of Fig. 10. However, the undulations do not completely disappear due to the high energetic cost of curvature walls which are bidimensional defects.

These results show that the defects of thin smectic films can also correspond to a mixture between focal conic domains, corresponding to the flattened hemicylinders, and curvature walls, located between the flattened hemicylinders, similarly to the hexagonal network described by Blanc and Kleman [2,9] in the lamellar/sponge system. However, in the cylindrical case, curvature walls appear to be of higher energy. Due to the cylindrical geometry, their length is larger. The disorientations between the layers along the wall correspond to larger values. Through the AFM measurements, θ_0 is in the range $10°-40°$, leading disorientations varying between 180° and $80°-20°$, instead of the fixed 26° in the lamellar/sponge system. The presence of such high energy defects is clearly imposed by the small thickness of the system. Following Blanc and Kleman [2], we can estimate the critical thickness associated with a replacement of focal conic domains by curvature walls between flattened hemicylinders. The energy of a focal conic domain can be written as $E_{FC}=\epsilon\pi KR$, R being the radius of the focal conic and ϵ being a constant of the order of 30, as inferred by Blanc and Kleman from their experimental results on toric focal conic domains, including the inner defect energy. The energy per unit area of a curvature wall without dislocation is $e_W=(2K/\lambda)(\tan\omega-\omega)\cos\omega$, λ being the smectic penetration

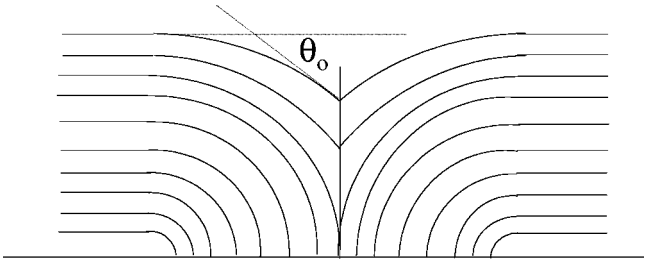

FIG. 16. Scheme of flattened hemicylinders with curvature walls between the hemicylinders. The corresponding curvature varies from 180° on the substrate to $2\theta_0$ at the interface in contact with air.

length (of the order of 3 nm in case of 8CB) and ω the half disorientation between smectic layers [2]. This leads to the following total energy of a wall of length $2R$ between two hemicylinders of thickness e:

$$E_W = \frac{4K \text{ Re sin } \theta_0}{\lambda} \int_{\theta_0}^{\pi/2} d\omega \left(\frac{1}{\sin \omega} - \frac{\omega \cos \omega}{\sin^2 \omega} \right)$$

$$= \frac{4K \text{ Re sin } \theta_0}{\lambda} \left(\pi/2 - \frac{\theta_0}{\sin \theta_0} \right)$$

with the elastic contribution of rotating smectic layers between the bidimensional curvature wall and the flattened hemicylinders equal to

$$2KR \left(-\pi/2 \ln \sin(\theta_0) - \int_0^{\pi/2-\theta_0} \omega \tan \omega \, d\omega \right).$$

In the case of an angle $\theta_0 = 20°$, the critical thickness, below which curvature walls become more favorable, is then $e_c = 0.37$ μm, indeed close to 0.35 μm, as obtained through optical microscopy measurements. Such an agreement confirms the validity of the hypothesis of presence of curvature walls between the flattened hemicylinders for small thicknesses.

The next step consists of introducing such defects energy in the previous energetical model in order to take into account the presence of defects between the flattened hemicylinders. However, this will also introduce two variables θ_0 and r_0 instead of only r_0. In order to extract from the model the unknown $\Delta\gamma_{MoS_2}$ and U values, precise values of θ_0 function of the thickness are then necessary. New x-ray diffraction experiments need to be performed for small thicknesses, in order to complete the model. The determination of $\Delta\gamma_{MoS_2}$ would allow in particular a comparison between the anisotropies of surface tension of different systems and an estimation of the specificity of smectic phases compared to nematic ones as well.

VIII. CONCLUSION

We determined the structure of smectic layers in a well defined frustrated geometry associated with antagonistic anchorings. We studied the deformations of thin smectic films by combining three different experimental techniques. X-ray diffraction revealed the continuous rotation of smectic layers between the interfaces. Optical microscopy results combined with x-ray results revealed the flattenned hemicylindrical structure in which smectic layers are concentrically stacked in quarters of cylinders joined by parallel layers. AFM observations, performed in the Tapping mode in a noncontact regime, revealed the presence of matter between the hemicylindrical structures, associated with focal conic domains for thicknesses higher than 0.35 μm and curvature walls of high disorientations for small thicknesses. Flat layers between rotating ones as well as curvature walls allow for a reduction of the high 8CB/air surface energy.

The thin deformed smectic films finally appear as organized in optical gratings formed by a mixture of 1D focal conic domains and curvature walls. The period is monitored by the complex competition between anchoring energies at air and on the substrate, defect, and rotating energies. The calculation of these different energies requires now a precise determination of the curvature wall geometry.

ACKNOWLEDGMENTS

We gratefully acknowledge Prof. C. M. Knobler for a careful reading of the manuscript and for useful suggestions.

[1] C. E. Williams and M. Kleman, J. Phys. Colloq. **36**, C1-315 (1975).
[2] C. Blanc and M. Kleman, Eur. Phys. J. B **10**, 53 (1999).
[3] T. P. Rieker, N. A. Clark, G. S. Smith, D. S. Parmar, E. B. Sirota, and C. R. Safinya, Phys. Rev. Lett. **59**, 2658 (1987).
[4] N. Vaupotic, M. Copic, and T. J. Sluckin, Phys. Rev. E **57**, 5651 (1998).
[5] I. Dozov and G. Durand, Europhys. Lett. **28**, 25 (1994).
[6] Y. Ouchi, Y. Takanishi, H. Takezoe, and A. Fukuda, Jpn. J. Appl. Phys., Part 1 **28**, 2547 (1989).
[7] E. Perez and J. E. Proust, J. Phys. (France) Lett. **38**, L117 (1977).
[8] J. B. Fournier, I. Dozov, and G. Durand, Phys. Rev. A **41**, 2252 (1990).
[9] C. Blanc and M. Kleman, Phys. Rev. E **62**, 6739 (2000).
[10] E. Smela and L. J. Martinez-Miranda, J. Appl. Phys. **73**, 3299 (1993).
[11] E. Smela and L. J. Martinez-Miranda, J. Appl. Phys. **77**, 1923 (1995).
[12] J. B. Fournier and G. Durand, J. Phys. II **1**, 845 (1991).
[13] K. Kocevar and I. Musevic, Liq. Cryst. **28**, 599 (2001).
[14] D. Beaglehole, Mol. Cryst. Liq. Cryst. **89**, 319 (1982).
[15] M. Hara, Y. Iwakabe, K. Tochigi, H. Sasabe, A. F. Garito, and A. Yamada, Nature (London) **344**, 228 (1990).
[16] D. Smith and W. Heckl, Nature (London) **346**, 616 (1990).
[17] E. Lacaze, P. Barois, and R. Lacaze, J. Phys. I **7**, 1645 (1997).
[18] E. Lacaze, M. Alba, M. Goldmann, J. P. Michel, and F. Rieutord, Appl. Surf. Sci. **175-176**, 337 (2001).
[19] J. P. Michel, E. Lacaze, M. Alba, and M. Goldmann, Surf. Sci. **507-510**, 374 (2002).
[20] E. Lacaze, M. Alba, M. Goldmann, J. P. Michel, and F. Rieutord, Eur. Phys. J. B (to be published).
[21] E. Lacaze, J. P. Michel, M. Goldmann, M. de Boissieu, M. Gailhanou, and M. Alba, Phys. Rev. E **69**, 041705 (2004).
[22] D. Davidov, C. R. Safinya, M. Kaplan, S. S. Dana, R. Schaetzing, R. J. Birgeneau, and J. D. Litster, Phys. Rev. B **19**, 1657 (1979).
[23] Y. Yoneda, Phys. Rev. **131**, 2010 (1963).
[24] G. H. Vineyard, Phys. Rev. B **26**, 4146 (1982).
[25] A. Primak, M. Fisch, and S. Kumar, Phys. Rev. Lett. **88**,

035701 (2002).
[26] C. Allet, M. Kleman, and P. Vidal, J. Phys. (Paris) **39**, 181 (1978).
[27] M. Tintaru, R. Moldovan, T. Beica, and S. Frunza, Liq. Cryst. **28**, 793 (2001).
[28] H. Schuring, C. Thieme, and R. Stannarius, Liq. Cryst. **28**, 241 (2001).
[29] M. G. Gannon and T. E. Faber, Philos. Mag. **37**, 117 (1977).
[30] M. J. Bradshaw and E. P. Raynes, J. Phys. (Paris) **46**, 1513 (1985).
[31] Z. Li and O. D. Lavrentovich, Phys. Rev. Lett. **73**, 280 (1994).
[32] M. Kléman and O. D. Lavrentovitch, Eur. Phys. J. E **2**, 47 (2000).
[33] B. Jerome, Rep. Prog. Phys. **54**, 391 (1991).
[34] M. Vilfan, A. Mertelj, and M. Copic, Phys. Rev. E **65**, 041712 (2002).
[35] J. E. Proust, E. Perez, and L. Terminassian-Saraga, Colloid Polym. Sci. **254**, 672 (1976).
[36] A. Buka, T. TothKatona, and L. Kramer, Phys. Rev. E **49**, 5271 (1994).
[37] C. Blanc, Ph.D. thesis, Université Paris 6, 2000.
[38] C. Blanc, Phys. Rev. E **64**, 011702 (2001).
[39] R. Meister, M. A. Halle, H. Dumoulin, and P. Pieranski, Phys. Rev. E **54**, 3771 (1996).
[40] C. Odin, J. P. Aime, Z. El Kaakour, and T. Bouhacina, Surf. Sci. **317**, 321 (1994).
[41] R. Bidaux, N. Boccara, G. Sarma, L. de Seze, P. G. de Gennes, and O. Parodi, J. Phys. (France) **34**, 661 (1973).
[42] M. Ambrozic, S. Kralj, and S. Zumer, Eur. Phys. J. E **8**, 413 (2002).